Automated analysis of stable operation in two-section quantum dot passively mode locked lasers

K. Brown[a], M. Fanto[a], D. Murrell[a], V. Kovanis[b] , Y.-C. Xin[c] and L.F. Lester[c]

[a]Air Force Research Lab, Electro-optical Components, Rome Research Site, 25 Electronics Pkwy, Rome, NY 13441
[b]Air Force Research Lab, Wright-Patterson AFB, OH 45433
[c]Center for High Technology Materials, University of New Mexico, 1313 Goddard SE, Albuquerque, NM 87106

ABSTRACT

In this paper, two-section mode-locked lasers consisting of monolithic quantum dot gain and absorber sections are studied as a function of absorber voltage, injected current to the gain region, and relative section lengths. We map the regions of stable mode-locking as measured by the electrical and optical spectra. A simple algorithm is presented that evaluates the quality of mode locking and allows automated characterization of devices. The relative advantages of increasing the absorber length compared to increasing the absorber reverse bias voltage are analyzed. Initial data indicate that doubling the absorber length from 1.4 to 2.8-mm in a 5 GHz repetition rate device increases the region of stable mode-locking by at least 25%, while increasing the absorber reverse bias can more than double the mode-locking regime. Nonetheless, in these devices, stable mode-locking over greater than a 100 mA bias range is realized with a grounded absorber making single bias control of a passively mode-locked semiconductor laser feasible.

Keywords: quantum dots, passive mode locking, semiconductor lasers

1. INTRODUCTION

In recent years, semiconductor lasers utilizing quantum dot active regions have been used to generate stable optical pulses, taking advantage of quantum dots' low line-width enhancement factor, low threshold, and wide gain bandwidth.[1,2,3] In many applications a pulsed source with an output tuned for transparency in silicon photonic materials is required. Additionally, these sources must have low timing jitter and be capable of peak powers greater than one Watt if they are to be used as transmitters in arbitrary waveform systems.

Of secondary interest is increasing the pulse repetition rate into the THz range by harmonic mode locking. One way to increase the repetition rate is to divide the laser into several sections and electrically isolate each section.[4,5] Each section can then be used as an absorber, gain, or passive region depending on the polarity and strength of the voltage bias and the amount of current injected. The versatility and flexibility of the multi-section layout should not be understated. It has been shown that pulse duration and output power are dependent on the specific positioning of the three types of section, and that certain configurations are clearly a better choice.[6] Further, precise positioning of the absorber can force the cavity to mode lock on high-order harmonics increasing the repetition rate.[6,7]

In this work we devise an automated method to map the mode-locking regions of several two-section devices and compare the size of these regions with respect to absorber length, absorber bias, and injection current. We also demonstrate an increase in the size of the mode-locked region with an increase in the number of quantum dot stacks in the gain region and show the increased number of stacks contributes to reducing gaps in the mode-locking maps.

Physics and Simulation of Optoelectronic Devices XV, edited by Marek Osinski, Fritz Henneberger, Yasuhiko Arakawa, Proc. of SPIE Vol. 6468, 64681M, (2007) · 0277-786X/07/$18 · doi: 10.1117/12.710845

2. EXPERIMENT

In this section we detail the test and evaluation of quantum dot diode lasers for mode-locking in various regions of absorber voltage bias and injection current. The lasers tested are all based on dots-in-a-well (DWELL^{TM}) technology originally developed by the Center for High Technology Materials (CHTM).[8] The devices tested have cavity lengths of 8 mm and absorber lengths of either 1.2 or 2.4 mm. All devices locked at the fundamental cavity rate of 5 GHz. The primary goal of this work was to create a laboratory where devices could be quickly evaluated and characterized with minimal personnel involvement. To this end, we designed a setup detailed below in Fig. 1.

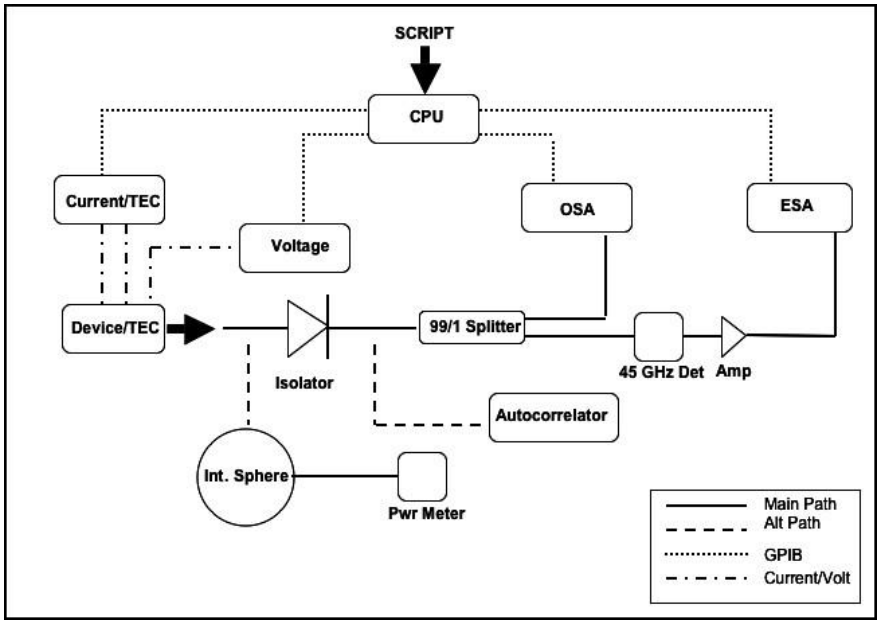

Figure 1. Experiment layout. Device output is coupled into polarization maintaining fiber or directly into an integrating sphere. OSA is optical spectrum analyzer, ESA is electronic spectrum analyzer, and TEC is temperature controller.

Each chip (containing up to 18 devices) was mounted to a TE cooler and maintained at a constant temperature of 25 degrees Celsius. An ILX LDC-3900 4-channel current source controlled both the TE cooler and the injection current. An Amrel PPS-1202 programmable DC power supply controlled the absorber bias voltage. Both the voltage ramp profile and the current ramp profile are controlled via a LabView script. The laser output is coupled into a single mode polarization maintaining lensed-tip fiber. An isolator is used to minimize feedback into the cavity of the device. The output of the isolator can be connected to a Femtochrome FR-103XL autocorrelator, an Ando AQ6317B optical spectrum analyzer, or a 50 GHz HP 8565E electronic spectrum analyzer. All equipment but the autocorrelator was remotely operated through the LabView script. To measure the average power, an Oriel 70451 four inch integrating sphere and Newport 883 IR detector were used. The integrating sphere was chosen over complicated coupling optics to ensure the highest possible accuracy when measuring the average output power of each device. The integrating sphere and detector were calibrated from a reference source.

Each data collection run was controlled via a LabView script. This script was executed via a graphical user interface that allowed the customization of each run to a specific device, or running the same current and voltage ramp profile sequentially to take an average on a single device. Depending on the resolution required and number of ramps, each device required 30 to 90 minutes to characterize. The data are stored in several text files for easy manipulation in MATLAB. The voltage and current resolution was 0.1 volts and 10 μA, respectively.

3. ALGORITHM AND ANALYSIS

In this section we describe the process of analyzing the raw data captured by the LabView script and how the data were transformed into meaningful mode-locking maps. To determine how well a device is mode-locked we analyzed the electronic spectrum of the devices' optical output. Strong upper harmonics indicate regions of good mode locking. We paid specific attention to the strength of the fourth harmonic (i.e., four times the cavity fundamental frequency of approximately 5 GHz). The electronic spectrum viewed over a 100 MHz span centered near the fourth harmonic quantitatively described the quality of mode-locking at a particular pair of injection currents and absorber bias voltages. In previous work at CHTM, a strong fourth harmonic correlated with jitter of less than 5 ps and pulsewidths less than 15 ps. We aimed to confirm this empirical result and expand the utility of observing the fourth harmonic by also looking at its shape. Observation of the higher harmonics was not possible due to their low signal-to-noise level.

In many cases where the mode-locking was strong, the peak of the fourth harmonic was 30 dB above the noise floor and was easily distinguished from incomplete mode locking by signal-to-noise ratio alone, as shown in Figure 3(a). A degraded mode-locked event is shown in Figure 3(b). However, the peak value of the fourth harmonic is an insufficient indicator of strong mode-locking and this simplified approach resulted in inaccurate mode-locking maps. To increase the accuracy of the mode locking map, we designed an algorithm that was able to successfully distinguish between the two cases with a low rate of false negative or positive "hits." Figure 2 is an outline of this algorithm.

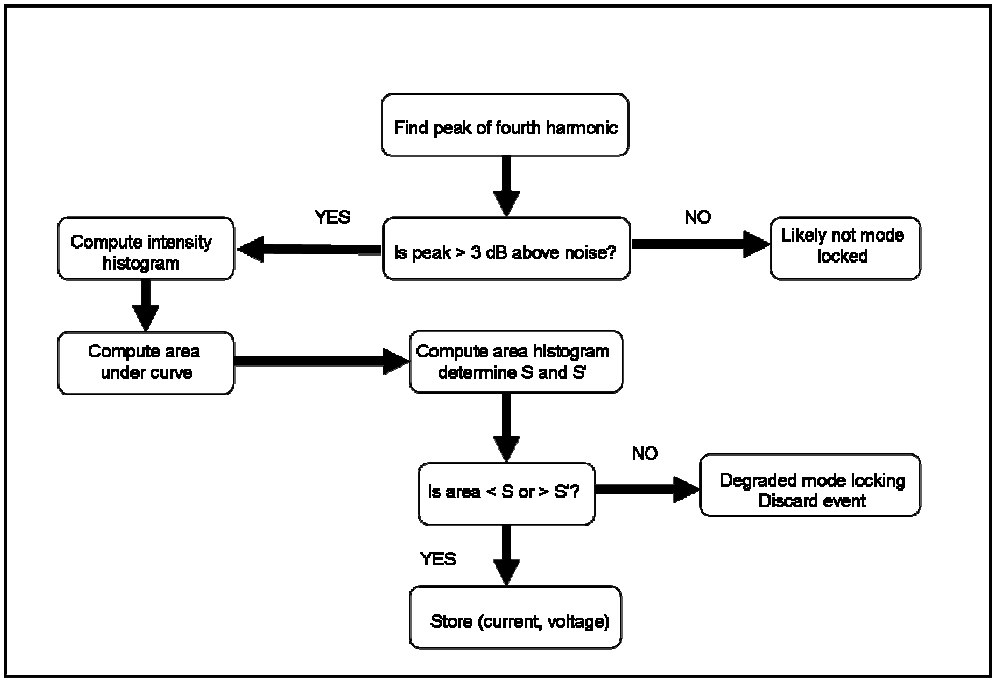

Figure 2. Algorithm for determining whether or not a particular ordered pair of absorber bias and injection current is mode locked. S and S' are chosen by analyzing the area histogram (see text). The algorithm allows performance analysis of a particular device in seconds, reducing the need for tedious manual comparison.

First, the algorithm determines the peak value of the fourth harmonic of each event. Next, it determines if the peak is greater than 3 dB above the noise floor. This is necessary to catch weak but sharp harmonic

peaks. The histogram of the electronic intensity spectrum is computed and the area under the curve for each voltage/current pair is calculated. The histogram contained 50 intensity bins that the data can fall in to. Figure 4 is a histogram signature of two different events. This depiction provided great insight into the quality of a certain event. In Figure 4, the data points representing the noise floor (about -73 dBm) are easily identified and filtered out. In Figure 4(a) and 4(b), the main peaks from both events are similar in shape and spectral composition. It is immediately apparent, however, that in Figure 4(b) a larger number of occurrences exist from approximately -63 dBm to -53 dBm. A degraded mode-locked event will have significantly more area under this part of the histogram than a strong mode-locked event. By comparing the magnitude to a known reference, an accurate comparison can be made.

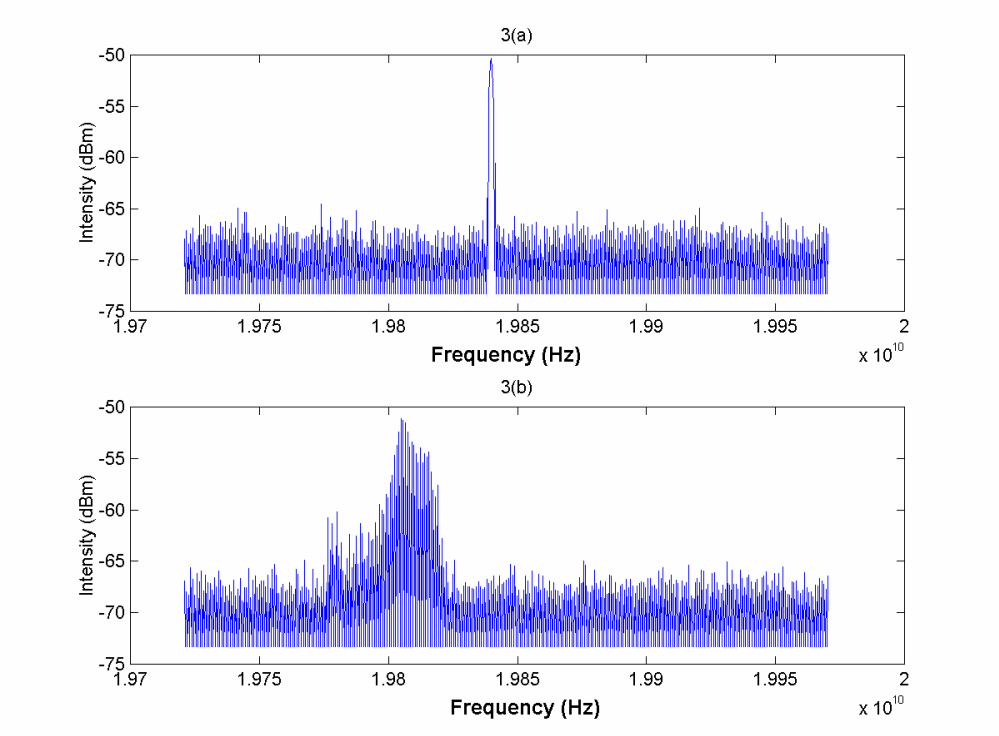

Figure 3. Electronic spectra of two different mode-locked events. 3(a) is the fourth harmonic output (about 19.85 GHz) during a strongly mode-locked event. 3(b) is the same output during a degraded mode-locking event. While the height of both peaks is well above the noise floor, the shape and intensity histogram determine the quality of the mode-locking.

To decide what intensity range to look for these extra occurrences, we calculated the histogram of the *areas* under the electronic spectrum of each event. In most cases, the choice of cutoff is obvious as the areas of the strongly mode-locked peaks congregated in a narrow range. In contrast, the occurrences of specific areas values in mode-locked peaks with significant degradation were spread out and always much larger than the area values of strongly mode-locked events. To clarify this point, strongly mode locked peaks have areas that ranged from 5-15 (arbitrary units) and the degraded mode-locked peaks had areas ranging from 20-100.The area histogram allows one to choose an area cutoff (S and S', representing upper and lower limits) for the algorithm and greatly reduces the rate of false negatives without a significant computational penalty.

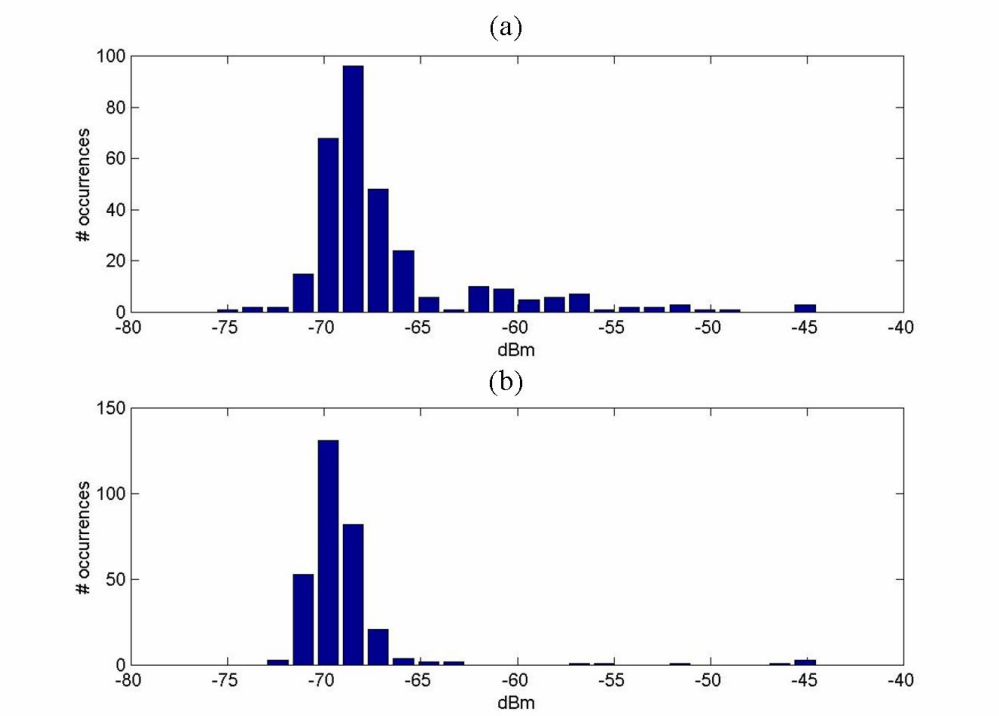

Figure 4. Intensity signature of degraded (a) and strong (b) mode locking. The broad envelope between -75 and -65 dBm is the random system noise. The data for the fourth harmonic peak falls between -65 and -45 dBm. Note the difference in the number of occurrences in the range from -63 dBm to -53 dBm. The significant difference in the area under the curve in this range allows the algorithm to easily distinguish a strong mode locked peak from an intense but degraded mode-locked peak.

Preliminary mapping efforts ramped injection current through a large range, often greater than 400 mA. This resulted in confusing and inaccurate maps showing gaps where a well mode-locked state should exist. We discovered that over such a large current range, thermally induced beam steering reduced the amount of coupled light into the fiber and caused the intensity of the fourth harmonic to drop below the noise. In order to prevent this from happening, we split each run into several 50 mA ramps and realigned the input fiber for peak power at the beginning of each run. This method greatly reduced false negatives and resulted in much more accurate maps.

4. EFFECT OF ABSORBER LENGTH

Once a suitable algorithm was developed to determine whether a mode locked event occurred, we characterized the effect absorber length had on the size and shape of the mode locked region. The results are graphically depicted in Figure 5 for two different lengths: 1.4-mm and 2.8-mm. The advantages and disadvantages of absorber length are discussed. The device tested was ZLG-414 which has a 6-stack quantum dot active region with 66% Al in the AlGaAs cladding layers and GaAs core waveguide. At most absorber bias voltages, the 2.8-mm absorber increased the range of injection current where mode-locking occurred by about 50%. This is due to the higher unsaturated loss and increased pulse shaping. The length of the absorber was found to play a critical role in suppressing nonlinearities that degrade mode locking. Nonlinearities express themselves by creating “gaps” in the mode-locking map. These gaps can be seen in Figure 5(b) following a small range of injection currents. For the 1.4-mm absorber, two gaps exist, one

from 275-300 mA and the other from 425-450 mA. In comparison, the 2.8-mm map lacks these features and demonstrates better control of these nonlinearities.

However, there are several tradeoffs using a long absorber. Increasing the absorber length was found to increase the threshold regardless of absorber bias. The increased unsaturated loss of the longer absorber restricts the maximum useable absorber bias voltage by about 40%. This decrease in absorber bias voltage limits the minimum recovery time and thus ultimately, the minimum pulse width. However, this may be compensated by the increased amount of pulse trimming that occurs in a longer absorber.

.

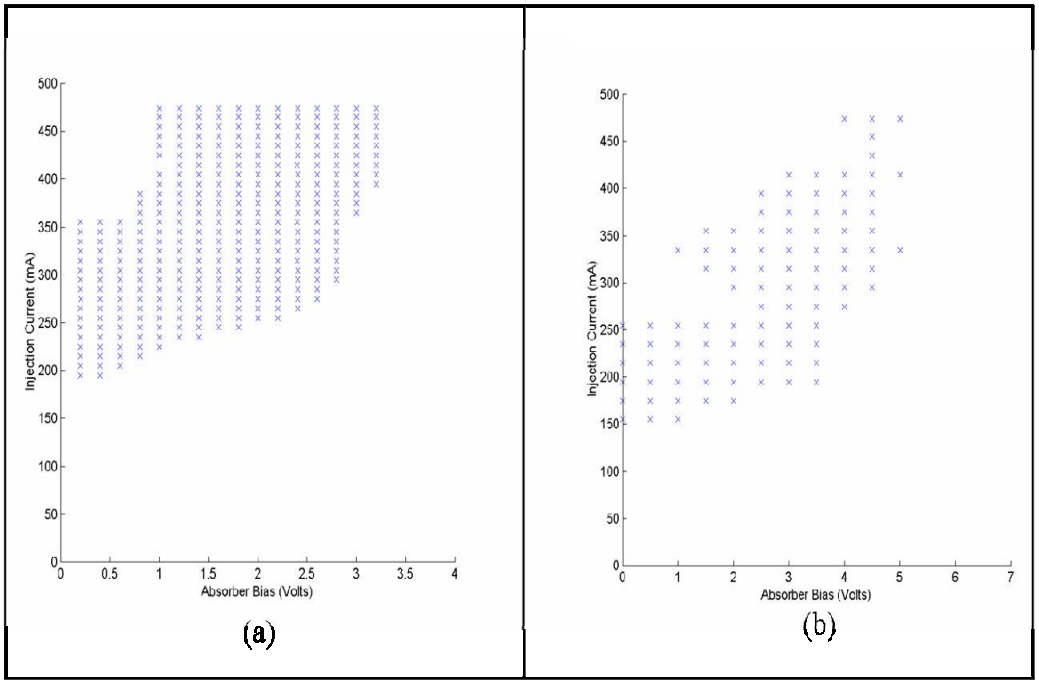

Figure 5. Mode-locked regions of ZLG-414 plotted as a function of injection current and absorber bias voltage for 2.8-mm absorber (a) and 1.4-mm absorber (b). This plot was generated using first harmonic information and only shows whether or not the device was mode-locked, but not how well. In (b) the deleterious effects of the shorter absorber express themselves as gaps in the mode-locking map. Note that mode-locking can also occur with a grounded absorber over an approximately 100 mA range.

5. MODE-LOCKING QUALITY

When evaluating promising devices, it is important to not only know where the device mode-locks, but also the quality of the mode-locking. As previously mentioned, the presence of a strong fourth harmonic in the electronic spectrum is an indication of good mode-locking. The algorithm described in Section 4 was used to generate the stability map of the devices in Figure 6, 7, and 8. The ZLG-839G devices (mapped in Figures 6 and 7) consists of a 6-stack quantum dot active region with 20% Al in the AlGaAs cladding layers and a GaAs core waveguide.

In Fig. 6, the mode-locking region was mapped as in Figure 5, but this time the algorithm filtered out degraded mode-locking. When the quality of mode-locking is taken into consideration, gaps are created. The two insets show electronic frequency spectra of events in these gap locations. The gaps at higher bias current correspond with the upper inset and the drop-out regions near threshold correspond to the lower

inset. The fact that the mode-locking quality fluctuates with erratic trends possibly indicates a sensitivity to residual optical feedback or nonlinearities that are not well understood at this time.

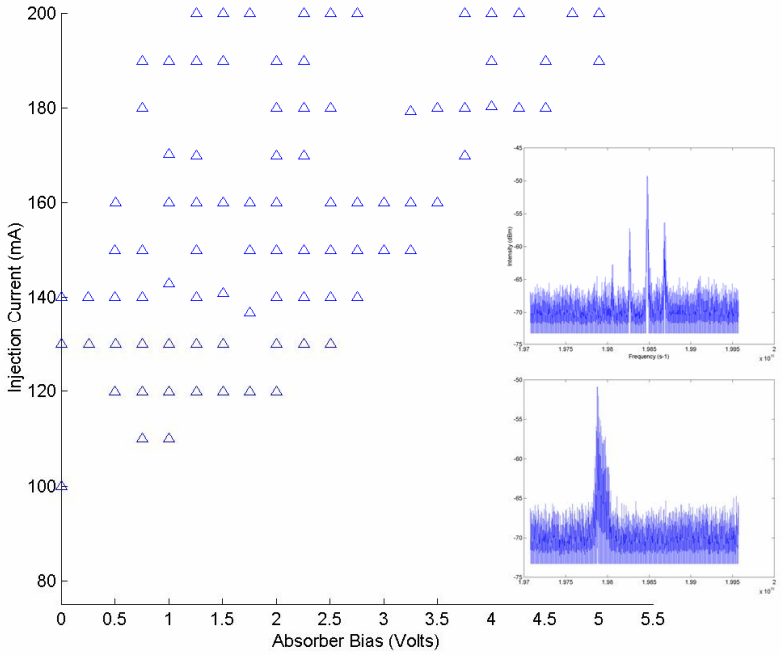

Figure 6. Mode-locking map of device ZLG-839G-17. The two insets are examples of degraded mode-locking present in the two gaps near the top of the plot. These empty regions are transition zones where strong mode locking becomes degraded as the current is lowered (at a fixed bias voltage) until strong mode locking reappears. This is not well understood and deserves more study.

The script used to control each run begins at high currents and low voltages and then proceeds to decrease the current until a minimum is reached, and then increase the voltage during the next cycle. For example, strong mode-locking was found at the beginning of one ramp cycle at 200 mA. The next current tested was 190 mA where the mode locking degraded and the electronic spectrum widened or became multi-peaked. At some lower injection current, the electronic spectrum narrowed and strong mode locking resumed until the lasing threshold was reached. This effect is not well understood and deserves more study.

In Figure 7 we demonstrate the effectiveness of the algorithm as a diagnostic tool. With many devices on a chip, some will not function properly and should be avoided. To manually determine which devices on a chip are worthy of further analysis would be time intensive and tedious. However, using the apparatus and algorithm described above, each device on a chip can be evaluated for performance by inspection. In Figure 7, the mode-locked map of device ZLG-839G-18 is shown. ZLG-839G-18 is theoretically identical to device ZLG-839-17 shown in Figure 6. Clearly though, ZLG-839G-18 is inferior to the ZLG-839G-17 in two ways. First, the maximum absorber bias in which mode locking occurs decreased by 23%. This ultimately limits the peak power of the device, and its usefulness in arbitrary waveform systems will be limited. Second, there are more regions of degraded mode locking where the electronic spectrum has widened (see inset).

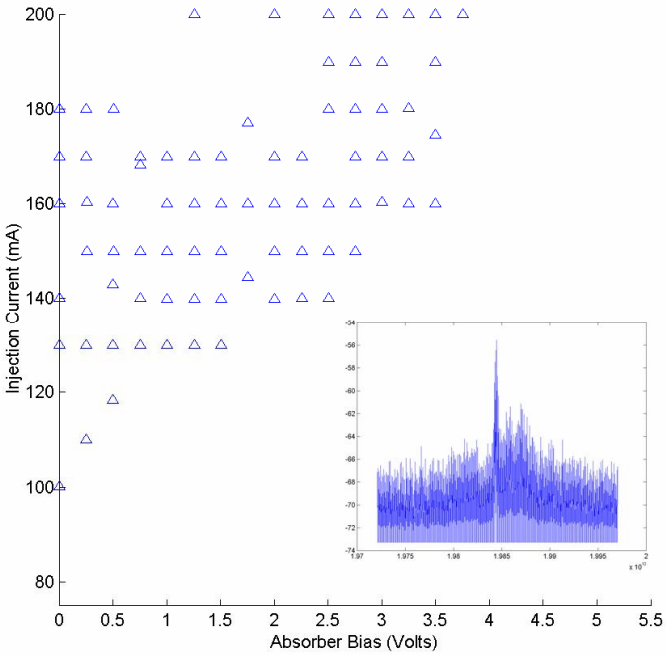

Figure 7. Mode-locking map of device ZLG-839G-18. This device is theoretically identical to ZLG-839G-17 but the algorithm demonstrates that ZLG-839G-18 is inferior. The inset shows the electronic spectrum of an degraded mode-locked event typical of the gap region. The culprit for this discrepancy is likely wafer or dot-density non-uniformity between the two devices.

Figure 8 shows the mode-locking map of device ZLG-967E. In contrast to device ZLG-839, this device consists of an 8-stack quantum dot active region with 20% Al in the AlGaAs cladding layers and a GaAs core waveguide. This device had a much larger mode-locked envelope than ZLG-839G while sharing many similar traits with respect to gaps indicating regions of degraded mode-locking. The gaps existed in similar places and were about the same size. Since the two chips are nominally the same with the exception of the number of quantum dot stacks, this result indicates that the larger number of quantum dot stacks increased the size of mode-locked region and also significantly reduces the gaps due to nonlinearities. It should also be noted that the differences between the two chips were not known at the time the mode-locking maps were generated. This demonstrates the effectiveness of the algorithm as a tool for evaluating device designs.

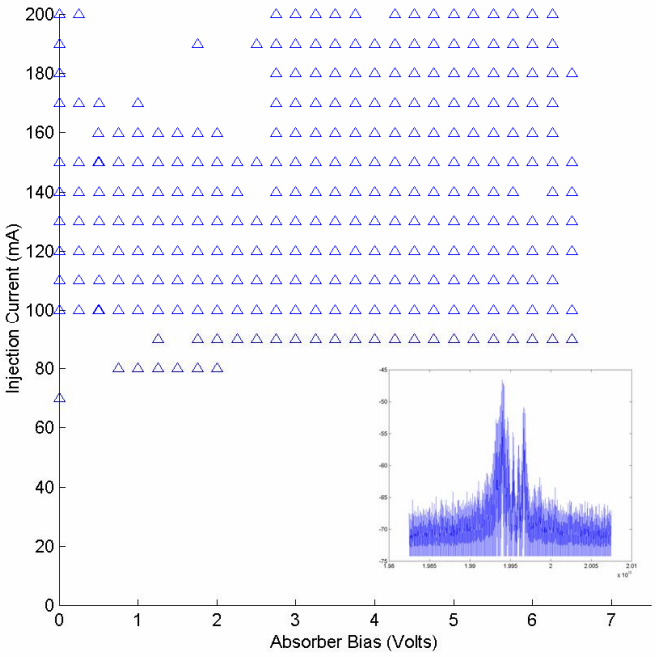

Figure 8. Mode-locking map of device ZLG-967E which has 33% more quantum dot stacks in the active region than ZLG-839G. The inset depicts the electronic spectrum in the gap near threshold. Compare the much larger mode-locked region to ZLG-839G in Figure 6. The increased number of quantum dot stacks significantly increased the size of the mode-locked region and decreased the instability gaps. Also note the larger number of injection currents where mode locking occurs with a grounded absorber.

6. SUMMARY

We demonstrate an effective tool for determining the size and shape of mode-locked regions for a quantum dot diode laser. This tool is completely automated via LabView and only relies on the electronic data collected from each device. We compare and contrast the effect of increasing the absorber length in a two-section device and show that this increases the region of mode locking over a range of injection current at a constant absorber bias. The deleterious effect of a short absorber is shown by the existence of large regions of degraded mode-locking. The longer absorber allows an expanded operating range over a constant absorber bias. We also demonstrate that increasing the number of layers of quantum dots significantly increases the size of the mode-locked region and increases the stability of mode-locking in general. An algorithm was developed to determine the quality of mode-locking. This provided a method to quickly determine a device's performance envelope and dismiss inferior devices thus saving the researcher considerable time.

Future work will concentrate on development of a rate equation model to understand the existence of the areas of degraded mode-locking. We propose to influence future designs of multi-section quantum dot lasers with special consideration given to absorber length, dot density, and wafer uniformity. The next version of the algorithm will integrate the pulse width and pulse jitter to further refine the mode-locking map.

This work was partially supported under AFOSR Award No. FA9550-06-1-0411 and AFRL Award No. FA8750-06-1-0085. The authors thank Zia Laser, Inc. for the use of their ZLG-series chips.

REFERENCES

1. T.C. Newell, *et.al.*, "Gain and linewidth enhancement factor in InAs quantum-dot laser diodes", IEEE Photon. Tech. Lett., vol. 11, no. 12, Dec. 1999.
2. M. Kuntz, G. Fiol, M. Lammlin, D. Bimberg, M.G. Thompson, K.T. Tan, C. Marinelli, R.V. Plenty, I.H. White, V.M. Ustinov, A.E. Zhukov, Yu. M. Shernyakov, A.R. Kovsh*,"*35 GHz mode-locking of 1.3μm quantum dot lasers", Appl. Phys. Lett. Vol. 85, p.843, Aug. 2004.
3. M.G. Thompson, C. Marinelli, X. Zhao, R.L. Sellin, R.V. Plenty, I.H. White, I.N. Kaiander, D. Bimberg, D-J. Kang, and M.G. Blamire,"Colliding-pulse modelocked quantum dot lasers", Electronics Lett. Vol. 41, no. 5 (2005)
4. L.Zhang, *et.al.,* "5 GHz Optical Pulses From a Monolithic Two-Section Passively Mode-locked 1250/1310 nm Quantum Dot Laser for High Speed Optical Interconnects," *Optical Fiber Communication Conference.Technical Digest.OFC/NFOEC*, vol. 3 2005
5. E.U. Rafaillov, M.A. Cataluna, W. Sibbett, N.D. Il'inskaya, Yu. M. Zadiranov, A.E. Zhukov, V.M. Ustinov, D. A Livshits, A.R. Kovsh, N.N. Ledentsov. "High-power picosecond and femtosecond pulse generation from a two-section mode-locked quantum-dot laser", Appl. Phys. Lett., Vol. 87, (2005)
6. Y.-C. Xin, V. Kovanis, A. L. Gray, L. Zhang, and L. F. Lester, "1.3-μm Quantum Dot Monolithic Multi-Section Passively Mode-Locked Laser," *IEEE LEOS 2006 Annual Meeting*, Montreal, Canada.
7. A. R. Rae, M. G. Thompson, R. V. Penty, I. H. White, A. R. Kovsh, S. S. Mikhrin, D. A. Livshits, I. L. Krestnikov, "Harmonic Mode-Locking of a Quantum-Dot Laser Diode," *IEEE LEOS 2006 Annual Meeting*, Montreal, Canada.
8. L.F. Lester, *et.al.*, IEEE Photon. Tech. Lett., vol. 11, no. 8, pp. 931-933 (1999)